LAWRENCE
LIVERMORE
NATIONAL
LABORATORY

UCRL-JRNL-205330

Melting of aluminum, molybdenum and the light actinides

M. Ross, L. H. Yang, R. Boehler

July 19, 2004

Physical Review B

Disclaimer

This document was prepared as an account of work sponsored by an agency of the United States Government. Neither the United States Government nor the University of California nor any of their employees, makes any warranty, express or implied, or assumes any legal liability or responsibility for the accuracy, completeness, or usefulness of any information, apparatus, product, or process disclosed, or represents that its use would not infringe privately owned rights. Reference herein to any specific commercial product, process, or service by trade name, trademark, manufacturer, or otherwise, does not necessarily constitute or imply its endorsement, recommendation, or favoring by the United States Government or the University of California. The views and opinions of authors expressed herein do not necessarily state or reflect those of the United States Government or the University of California, and shall not be used for advertising or product endorsement purposes.

Melting of aluminum, molybdenum and the light actinides

Marvin Ross[1],Lin H. Yang[1] and Reinhard Boehler[2]

1.Lawrence Livermore National Laboratory, Livermore, CA 94551, USA
2.Max-Planck-Institute fur Chemie, Postfach 3060, 6500 Mainz, Germany

Abstract

A semi-empirical model was used to explain why the measured melting curves of molybdenum, and the other bcc transition metals, have an unusually low slope (dT/dP~0). The total binding energy of Mo is written as the sum of the repulsive energy of the ions and *sp*-electrons (modeled by an inverse 6th power potential) and the d-band cohesive energy described by the well known Friedel equation. Using literature values for the Mo band width energy, the number of *d*-electrons and their volume dependence, we find that a small broadening of the liquid *d*-band width (~1%) leads to an increase in the stability of the liquid relative to the solid. This is sufficient to depress the melting temperature and lower the melting slope to a value in agreement with the diamond-anvil cell measurements. Omission of the *d*-band physics results in an Al-like melting curve with a much steeper melt slope. The model, when applied to the f-electrons of the light actinides (Th-Am), gives agreement with the observed fall and rise in the melting temperature with increasing atomic number.

I. Introduction

Recent advances in the application of laser-heated diamond-anvil cells (DAC) to the study of melting now enable simultaneous pressure-temperature measurements to be made in the megabar pressure range to 3000 K to 4000[1-4]. In the case of transition metals the advances have lead to the discovery of unusually low melting slopes (dT/dP~0) for the bcc metals, particularly in Groups VA and VIA of the Periodic Table[3-4]. These results are at odds with conventional wisdom that melting temperatures should rise continuously with increasing pressure [5]. However, new measurements for Ta made at the Advanced Photon Source (APS)[4], and using x-ray diffraction to detect melting, have confirmed the earlier results. The original purpose of this report is to offer a theoretical explanation as to why the transition metal melting curves have unusually low melting slopes. Mo was chosen as the test case for transition

metals because it has the smallest measured melting slope of that group, and thus provides the most severe test. Subsequently, it became apparent that the same physics applied to the light actinides.

Conceptually, the paper first considers Al as the prototypical nearly free electron *sp* metal and is modeled here by employing the inverse-sixth power repulsive potential. We then determine the consequence of adding *d*-electrons by building on the earlier work of Ducastelle [6] and Pettifor [7] that the total binding energy of a transition metal may be written in the form, $U = U_{rep} + U_{d\text{-}band}$. U_{rep} is the repulsive contribution of the ions and *sp*-electrons and $U_{d\text{-}band}$ is the cohesive energy of the d-band.

The equation of state for U_{rep} is first developed in Section II and applied to Al in Section III. In Section IV the $U_{d\text{-}band}$ is included in the total energy by using the Friedel equation[8], and the model is applied to Mo. The results of melting calculations are discussed in Section V.

II. Inverse-6 equation of state

The equations of state (EOS) for systems interacting via purely repulsive inverse power potentials,

$$\phi(r) = B/r^n, \qquad (1)$$

have been studied extensively by computer simulations for the hard sphere (n=∞), n=12, 9, 6, 4 and the one component plasma (n=1) [9,12]. An important simplifying feature of this potential is that the excess Helmholtz free energy, and all of the thermodynamic properties can be expressed as a function of a single parameter, the scaled inverse temperature;

$$\Gamma_n = \beta B/(a)^n. \qquad (2)$$

$\beta=1/NkT$, a is the Wigner Seitz radius given by $4\pi n_o a^3/3=1$ and n_o is the atom number density.

The inverse 6th power is of special interest here because previous work has shown that potentials near this power best represented the ab-initio liquid calculations of Al [13] and Fe[14] and served as a reference system for calculating the excess free energy needed for high pressure melting studies.

An exact analytic determination of the fcc and bcc free energies, including the first order anharmonic term, has been reported by Dubin and DeWitt [10] for the cases n=1 to 12. The expression for the excess solid free energy is,

$$\frac{F_e^s}{NkT} = M\Gamma_n + \frac{3}{2}\ln\left\{2\left[\frac{3}{4\pi}\right]^{n/3}\Gamma_n\right\} + 1 - S_H - \frac{A_1}{\Gamma_n} \qquad (3)$$

M, S_H and A_1 are the Madelung term, excess entropy and first-order anharmonic constants respectively. Values of these parameters for the inverse power potential are tabulated [10]. $M\Gamma_n$ is the Madelung energy, or the energy of the static lattice. While the terms S_H and A_1 are small, they determine the relative stability of the two solid structures near melting. The thermal internal energy, is related to the excess free energy by $U_{th}/NkT = -\partial\left(F_e/NkT\right)/\partial\Gamma$.

The results of Monte Carlo simulations for the excess liquid energy (U_e) [8] have also been fitted [9] to analytic functions of Γ_n:

$$U_e/NkT = M\Gamma_n + U_{th}/NkT \qquad (4)$$

$U_{th}/NkT = b\Gamma_n^{1/4} + c$ is the thermal energy. The excess Helmholtz free energy is

$$F_e^l/NkT = M\Gamma_n + 4b\Gamma_n^{1/4} + cLn(\Gamma_n) + d. \qquad (5)$$

In the case of the inverse 6th potential, b=0.9267 and c=-0.584. d =is a constant of integration which must be determined for solid-liquid phase transitions.

The 6th power potential appears to be roughly the border separating the stability range of bcc and fcc phases at melting. Hoover et al. [15], determined that for n=6, the fcc lattice is the minimum energy structure, while the looser packing of the bcc solid makes the entropy higher and favors the stability of this phase at higher temperature and near the melting. Laird and Haymet [11] have found a smaller region of bcc stability for n=6 than did Hoover et al.

More recently, Dubin and DeWitt[12]have determined that fcc, and not bcc, is the stable phase at melting for the n=6 and stiffer potentials. However, despite these differences there appears to be a general agreement that for values of n ≤ 6, bcc is the stable crystal structure at melting and occupies an increasingly larger portion of the phase space with decreasing values of n. In the case of the one-component plasma (n=1), bcc is the only stable phase below the melting temperature. Dubin and DeWitt suggest that the apparent discrepancies for n=6 follows from the neglect of higher-order

anharmonic corrections which become important near melting and allow that the fcc-bcc-liquid triple point is near n≈6.

It is now necessary to determine a set constants in the free energy equations (3) and (5) that are in reasonably agreement with the phase diagrams predicted by L-H and D-D. Since D-D limited their calculations to the fcc-bcc phase transition, while L-H also calculated the solid-liquid transition for both structures, we used the L-H values of $\square_S$ and $\square_L$, the solid and liquid parameters at melting and freezing respectively to adjust two of the constants .

In the case of fcc melting L-H found $\square_s$ and $\square_L$ to be 95.34 and 92.98 respectively. In order for our model to predict these values we used the liquid constants *b* and *c* cited above in (5) and set *d* (=2.8405) to fit the L-H excess liquid free energies. For the fcc free energy we used the parameters of D-D, S_{Hfcc}=-1.6585 and A_{1fcc} = 0.416.

To fit the L-H bcc melting parameters, 94.52 and 92.17, we used the same liquid model as in fcc melting, but adjusted the value of S_{Hbcc} in (3) given by D-D from –1.6585 to –1.586. This step is reasonable since D-D, as noted above, suggest discrepancies may have followed from the neglect of higher-order anharmonic corrections.

Considering the closeness of the predicted bcc and fcc melting parameters $\square_S$ and $\square_L$, these adjustments in fact played only a negligible role in the present study. But they provide some measure of satisfaction by allowing us to treat Al as fcc, and Mo as bcc .

III. Application to Aluminum

In order to apply the inv-6 equation of state to the melting of Al two approximations were made.

First, we replaced, the Madelung energy in equations (3-5) with the room temperature isotherm determined from diamond-anvil-cell measurements and fitted to the Birch-Murgnahan (BM) equation[16], corrected to their 0 K values. The excess free energy, total energy and pressure for each phase may be expressed as,

$$F_e = U_{BM} + F_{th\_inv6}\,, \tag{6}$$

$$E = U_{BM} + 1.5NkT + U_{th\_inv6}, \tag{7}$$

and

$$P = P_{BM} + \frac{NkT}{V} + \frac{n}{3}\frac{U_{th\_inv6}}{V}. \tag{8}$$

The second approximation involves determining the value of B in the potential (1). Vocadlo and Alfe calculated the melting curve for fcc aluminum employing density functional theory molecular dynamics and an inverse-6.7 power potential reference system with B=247 eV-cm$^{6.7}$, which best represented their liquid simulations [13]. By using the value of B=227 eV-cm^6 in (1) we are able to calculate a melting curve and Hugoniot that are in excellent agreement with melting measurements made in a laser-heated DAC [2].

The melting curves shown in Fig. 1 were calculated by two methods. In the first we utilized the scaling properties of the inverse-power potentials. By using Eq. 2, a set of melting temperatures and volumes could be chosen such that γ_S=95.34 for the solid, and γ_L=92.98 for liquid freezing. The calculated pressures appear as the two parallel curves, the lower curve being the solid melting curve. In a second method the melting point was determined at a given temperature by calculating the difference in the solid and liquid Helmholtz free energies, ΔF, at a series of volumes and then determining the volume at which ΔF=0. The pressure of the transition can be estimated by averaging the pressures of the two coexisting phases at the volume where ΔF=0. This method is useful for those cases, such as metals, where the volume change across the transition is very small, about 1.3% in the case of Al. The melting obtained using this second method is

not plotted, but lies, as it should, between the solid melting and liquid freezing curves determined using the first method.

The solid and liquid Hugoniots shown in Figs. 1 and 2 were calculated by satisfying the equation

$$E - E_o = 0.5(P + P_o)(V_o - V), \qquad (9)$$

where the subscripted variables are initial conditions in the solid at 298 K. The melting and freezing curves, shown in Fig. 1, cross the calculated Hugoniot at 120 GPa and 150 GPa respectively, in good agreement with the experimentally determined values of 125 GPa and 150 GPa. The shock melting pressures shown were determined experimentally from breaks in the shock sound velocity, but the temperature, not measured, had been estimated using the Grüneisen model [17].

IV Molybdenum

Molybdenum melts from the bcc phase at 2890 K. It is known to be stable in this structure at room temperature to a pressure of at least 416 GPa [18]. The stability of the bcc phase relative to close-packed is accounted for by a relative gap in the electron density of states (DOS) near the Fermi energy [19,20]. The driving force for a transition to hcp at higher pressure is believed to be a pressure-induced s-p to d electron transfer[21,22].

There is experimental and theoretical evidence which shows that upon melting changes occur in the atomic ordering of liquid Mo, and other bcc transition metals, which influence the valence electronic structure. Since it is well known that the bcc and fcc structures of transition metals have electron density of states (DOS) which differ significantly [21,22], then it should be expected that the melting of the 8-fold coordinated bcc structure to a more closely-packed liquid structure will lead to changes in the DOS. Time resolved photoelectron spectroscopy measurements for these metals show changes in the DOS in the solid and liquid which reflect the changes in atomic ordering from bcc to a close-packed-like ordering[23-25].

Ab-initio molecular dynamics simulations for open-shell transition metals also predict changes from a bcc structured DOS in the solid, with peaks and valleys, to a smoothed DOS in the liquid [26,27,28]. In contrast to the open-shell transition metals, the DOS of Cu, which has a filled d-band changes only slightly upon melting[28,29].

In effect, experiment and theory tell us that upon melting, both the atomic and the electron system in an open shell transition metal undergo a structural rearrangement. The significance of these results for melting is that, while the free energy changes resulting from atomic reordering are treated quite naturally by the statistical mechanical models, the differing contributions of the solid and liquid d-electron systems must also be considered.

A. Friedel model

We extend our Al model to Mo by writing the excess free energy of the solid and liquid phases as the sum of contributions from the BM static lattice, the inv-6 potential thermal free energy, and add the d-band cohesive energy.

$$F_e^s = U_{BM} + F_{th\,inv6}^s + U_{d\,band}^s \,, \tag{10}$$

and

$$F_e^l = U_{BM} + F_{th\,inv6}^l + U_{d\,band}^l \,. \tag{11}$$

For the d-band cohesive energy, $U_{d\text{-}bond}$, we employ the well known Friedel model [8]

$$U_{d\,band} = -\frac{W}{20} n_d (10 - n_d) \,. \tag{12}$$

W is the bandwidth and n_d is the effective number of d-electrons per ion. Since this term is temperature independent the thermal properties determined by the inv-6 EOS remains unaffected.

The Friedel model has proven successful in describing the variation of the cohesive energy of transition metals and their alloys with the filling of the d-band [30]. The cohesion is a maximum at the middle of a series (near Mo) when all the bonding states are filled and the anti-bonding states are empty. The contribution of the Friedel term to the pressure is then

$$P_{d\,band} = \frac{\partial W}{\partial V} n_d (10 - n_d)/20 \,. \tag{13}$$

The volume dependence of W has been described by, $W = W_o (R_{WS}^o / R_{WS})^n$, where W_o and R_{WS}^o correspond to the equilibrium band width and Wigner Seitz radius. n is a parameter obtained from electron-band theory calculations. Since the function W increases with decreasing volume, $P_{d\text{-}band}$ decreases with increasing compression. Values for W_o and n_d and n have been determined metal across the transition series. For bcc Mo, Pettifor [31] has calculated values of W_o=9.5 eV and n=4.3. We assume that the liquid phase can also be treated using the Friedel model, but with slightly different electronic properties.

Since the DAC solid isotherm, as represented by the BM fit, already includes the U_M and $U_{d\text{-}band}$ terms we avoid double counting and rewrite (10) and (11) as

$$F_e^s = U_{BM} + F_{th\_inv6}^s \,. \qquad (14)$$

$$F_e^l = U_{BM} + F_{th\_inv6}^l + \Delta U_{d\_band}^{l-s} \,. \qquad (15)$$

where $\Delta U_{d\_band}^{l-s} = (U_{d\_band}^l - U_{d\_band}^s)$ is the change in d-band cohesive energy going from the solid to liquid phase. The $\Delta U_{d\_band}^{l-s}$ term, which is small, but essential in the case of melting, enters as a perturbation.

B. Melting

Since there is little in the way of data for W_o and n_d available for liquid transition metals we assume that the liquid is effectively a close-packed fcc-like system. We rely on Moriarty's [21] calculation for estimates of n_d for bcc and fcc Mo calculated over a two-fold range in density. Moriarty found that n_d increased from about 4.2 electrons at normal density to about 4.72 at two-fold compression and that fcc had an n_d higher by about 0.1 electrons. To the extent that the liquid coordination number may be fcc-like we assume that the fcc values approximate those of the liquid. Since the parameter n increases with increasing n_d, then n must increase upon melting. A trial value of n=4.4, increased from 4.3 in the solid, was set for the liquid. A value for B, of 400 eV-cm^6, was obtained for the inverse-6 potential (1) by requiring that the normal melting point for Mo approximate the experimental value of 2890 K.

Melting points were obtained at a given temperature by calculating the difference in the solid and liquid Helmholtz free energies,

$$\Delta F = F_{th\_inv6}^l - F_{th\_inv6}^s + \Delta U_{d\_band}^{l-s} \qquad (16)$$

at a series of volumes and then determining the volume at which $\Delta F=0$. Fig. 3 shows the DAC measurements, the melting curves calculated by including and omitting the $\Delta U_{d\_band}^{l-s}$ term, and the calculated solid and liquid Hugoniots. The melting curve calculated by omitting the $\Delta U_{d\_band}^{l-s}$ term is in agreement with the predictions made by Moriarty [21], using pair potentials, and by Burakovsky et al.[32] using a Lindemann-like scaling model.

The melting curve calculated by including the ΔU^{l-s}_{d-band} term in (16) is in good agreement with the DAC measurements which show a slow rise in the temperatures up to 40 GPa with a flattening of the melting slope to $dT/dP \sim 0$ above that pressure. But above 90 GPa the model predicts that the temperatures begin to decrease and cross the solid Hugoniot near 181 GPa and 2639 K. The predicted decrease is possibly due to our limited knowledge of the Friedel model parameters at high density. The appearance of negative melting slopes in *d*-electron systems is well known and reviewed below in Section IV. However, by lowering the value of n slightly, from 4.4 to 4.39, the melting temperature near 220 GPa could be raised from 2205 K to 3011 K.

Plotted in Fig. 4 are $(F^{l}_{th-inv6} - F^{s}_{th-inv6})$ and ΔU^{l-s}_{d-band} at a series of temperatures at 75 GPa. Melting occurs at $\Delta F = 0$. The contribution of ΔU^{l}_{d-band} at this pressure is 0.128 eV/atom, which is about 1% of W. This reduction in the liquid free energy, even while numerically small , leads to a decrease in the melting temperature from 4942 K to 3170 K. The associated pressure drop is small, -5 GPa, but not negligible.

D. Electron density of states (DOS)

To better understand the solid and liquid structural properties near these conditions first-principles molecular dynamics simulations were performed for 54-atom Mo systems in the solid (at 3459K) and liquid (at 4960K) states in a periodic box, respectively. Plane-wave pseudo-potential method was used for the electronic structure calculation while the ionic trajectories were proceeded by the classical equation of motion. At each time step, the ionic positions were determined using the Hellman-Feynman forces obtained from electronic structures calculation in which the Bohn-Oppenheimer approximation is applied. The initial configurations for the 54-atom solid and liquid states were generated based on interatomic potentials derived from the modeled generated pseudo-potential theory (MGPT) [21,26]. The systems were equilibrated for 15 pico-seconds using MGPT potentials and then passed on to the first-principles MD calculations where the systems were further equilibrated for 0.5 ps and then ran for 3-4 pico-seconds to gather statistics.

Fig. 5 shows the calculated electron density of states (DOS) for liquid and solid Mo made at temperatures of 4956 K and 3459 K respectively. While the plots may have only a semi-quantitative significance they do indicate that the DOS in the liquid is smoother and broader than in the solid, leading to a larger value of W for the liquid.

The data in Fig. 5 implies that W is lower in the liquid by about 0.3 eV/atom. These results are consistent with those of Moriarty that showed the melting of the solid led to about a 0.3 eV/atom lowering of the Fermi energy.

D. Comparison with transitions reported in shock experiments.

Returning to Fig. 3, an extrapolation of the experimental melting measurements shows that it crosses the Hugoniot near 210 GPa and 3200 K. This is in excellent agreement with the pressure at which a break in the shock sound velocity was observed by Hixson et al. [33] and had been attributed to a bcc-fcc transition. In addition to the transition at 210 GPa, Hixson et al.[33] observed a second break in the shock sound velocity near 390 GPa and a calculated temperature near 10,000 K, which they attributed to melting of the bcc solid.

At 210 GPa and 3200 K, the pressure and temperature at which the Friedel model solid melting curve crosses the Hugoniot has the value of □~200. This high value is a consequence of the large depression in the melting temperature caused by the *d*-electrons and suggests that the melt is highly viscous. If the second break in the experimental shock data is real, we speculate that it may represent the transition from the viscous fluid to a normal liquid, but at a temperature much below 9000 K.

Evidence for the presence of a highly viscous state in transition metal melts has been reported by Brazhkin and Lypkin [34]. They carried out quenching experiments on transition metal melts for which an inspection of the grain size suggested strongly that the melts are very viscous and that the viscosity grows considerably along the melting curve. Brazhkin and Lypkin note that this appears to be the case in Fe providing some basis to the theory that the liquid in the Earth's core is viscous.

V. Melting of the actinide metals.

The chemical bonding in transition metals, and light actinides Th to Pu, are known to have strong similarities in that transition metal bonding is due to delocalized *d*-electrons and the light actinides by delocalized *f*-electrons. Bonding in the heavy actinides (Am and beyond) are characterized by more localized *f*-orbitals. Pu is located at the border of the light and heavy actinides. The unusual room temperature structures of the light actinides are believed due to the *f*-electron character [35].

Two related properties of the light actinides are particularly note worthy. The ambient melting temperatures of the light actinides and their alloys are anomalously low and decrease starting from Th, reaching a minimum near Pu, then rise for the heavier actinides [36]. To explain the anomalously low melting points of light actinides Kmetko and Hill [37] suggested that the angular dependence of f-electron wave-functions favored bonding in the liquid rather than the bcc phase. In a general sense, this is consistent with the view of transition metal melting that we have developed in this report.

The equilibrium room temperature volumes decrease from Th to a mininum at Pu then rise to Am and Cm [38]. Johannson and Skriver [39], explained this trend as being directly related to the increase in f-electron bonding with calculations using a simple model, similar to ours, which included the Friedel expression to calculate the *f*-band energy.

Rather than calculate the ambient melting temperatures specifically for each of the light actinides, we constructed a "hypothetical light actinide" series by simply adding f-electrons to thorium which, like all of the light actinides, melts from the bcc structure. Th is often considered as a transition metal with small f-character and a rather broad band of unoccupied 5*f* states above the Fermi level. By increasing the f-electron occupancy systematically we are able to simulate roughly the change in melting temperature across the light actinide series.

The theoretical model is the same as used in the preceding Section, except the Friedel term is written for *f*-bands ,

$$U_{f\text{-}band} = -\frac{W_f}{28} n_f (14 - n_f), \qquad (17)$$

with the remaining expressions for the pressure and free energy unchanged. For W_f, the f-band width, we use the simple formula and parameters employed by Johannson and Skriver[39], $W_f = W_f^o(V_o/V)^2$,where W_o and V_o correspond to the equilibrium band width and volume respectively. n_f, is *f*-electron occupation number. W_o = 3.6 eV.

The Birch-Murgnahan fit to the lattice pressure and energy came from the work of Bellussi et al[40]. We retained the use of the inverse 6th power potential with a value for B = 1050 eV-cm^6 and fit the melting point of thorium by using an n_f occupation number of 0.4. Wills and Eriksson [41] calculated that for Pa and U the fcc lattice has an *f*-electron occupancy about 1.5 to 5 % higher than for bcc. In the melting calculations described we chose an intermediate value, that the n_f in a close-packed liquid was higher by 1.025 than in the bcc solid.

Melting points were determined, as in earlier Sections, by calculating the difference in the solid and liquid Helmholtz free energies, at a series of volumes, at a given temperature by and then determining the volume at which ΔF=0. Fig. 7 shows the calculated ambient melting temperatures and the experimentally determined points plotted as a function of the *f*-electron occupancy. The *f*-electron occupancy of the experimental data was taken from the theoretical values reported by Soderlind et al. [42].

The predicted melting temperatures of our "hypothetical light actinide" are in good qualitative agreement with experiment. The model predicts a decrease in the melting temperature with increasing f-electron character, with a minimum near 3-4 *f*-electrons compared to the experimental 4-5 *f*-electrons.

VI. Discussion

In addition to transition metals and actinides, the association of low melting slopes with *d*-electron character is widespread. It is well known that in the case of the alkali and alkaline-earth metals the pressure induced increase of the *d*-electron occupation number causes a flattening of the potassium melting curve above 4 GPa and the appearance of complex structures in Ba, Sr and Ca[43]. In the case of Rb and Cs, negative melting slopes (dT/dP<0) lead to a temperature minima and maxima below 10 GPa[44]. In effect, pressure transforms the heavy alkali and alkaline metals to early

transition metals. The low melting slopes of the bcc transition metals, with high binding energies, represent the limiting cases of this trend.

The influence of d-electrons on melting at high pressure is nicely provided in Fig. 6 by a comparison of Al[2] and Mo[3] with Mg[43]. All three melting curves were measured at the same laboratory. The melting curve of Mg which, like Al, is a nearly free electron polyvalent metal, follows that of Al up to the transition pressure of 50 GPa. Above that pressure the melting slope of Mg decreases and bends parallel to the melting curve of Mo while the Al melting curve continues to rise. At room temperature, Mg transforms from hcp to bcc at 50 GPa [45] while Al remains fcc up to 220 GPa, the highest pressure for which measurements were made [16]. Theoretical calculations have shown that the increase in d-character is responsible for these transitions [46]. This suggests that the Al melting slope will also show a decrease near its fcc-bcc transition pressure.

In summary, the melting of transition and actinide metals differs profoundly from the case of rare gases and simple nearly free electron metals, such as Ar and Al, where the electronic structure and effective inter-atomic forces remain unchanged upon melting. Improvements in the theory will require a more detailed understanding of the liquid electronic properties.

Acknowledgments

Work by MR and LHY was performed by the University of California under the auspices of the US DOE by the Lawrence Livermore National Laboratory.

Work by MR and LHY was performed under the auspices of the U.S. Department of Energy by University of California, Lawrence Livermore National Laboratory under contract No. W-7405-Eng-48.

References

1) R. Boehler, *Nature (London)* **363**, 534 (1993).

2) R.Boehler and M. Ross, *Earth Planet. Sci. Lett.* **153**, 227 (1997).

3) D. Errandonea, et al. *Phys. Rev. B **63**,* 132104 (2001).

4) D. Errandonea, et al. *J. Phy.:Condens. Matter* **15**, 7635 (2003).

5) L. Vocadlo, et al. *J. Chem. Phys.* **120**, 2872 (2004); *Phys. Earth Planet. Interiors*, **140**, 101, (2003).

6) F. Ducastelle, *J.Phyique,* **31**, 1055 (1970).

7). D.G. Pettifor, *"Bonding and Structure of Molecules and Solids"*, (Clarendon Press, Oxford, 1995).

8) J. Friedel, in *The Physics of Metals* I, J. Ziman, ed. (Cambridge Univ. Press, Cambridge, 1969), p.340. Also see, J.A. Alonso and N.H. March *"Electrons in Metals"*,(Academic Press, London, 1989).

9) Hoover et al. *J.Chem. Phys*. **52**,4931 (1970*); ibid* **55**, 1128, (1971).

10) H.E. DeWitt, *"Strongly Coupled Plasmas (1978)",* ed. G. Kalman and P. Carini (Plenum, New York, 1979) p.81.

11) B.B. Laird and A.D.J. Haymet, *Mol. Phys*. **75**, 71 (1992).

12) D.H.E. Dubin and H. DeWitt, *Phys. Rev.* B **49**, 3043 (1994).

13) L. Vocadlo and D. Alfè, *Phys. Rev.* B **65**, 214105 (2002).

14) D. Alfè, G. Kresse and M.J. Gillan, *Phys. Rev*. B **61**, 132 (2000).

15) Hoover et al. *J.Chem. Phys.* **56**, 2207 (1972).

16) Greene et al. *Phys. Rev. Lett***. 73**, 2075 (1994).

17a) J.W. Shaner et al., in *"High Pressure Science and Technology*", eds. C. Homan, R.K. MacCrone, E. Whalley (North Holland, Amsterdam,1984) pp137-141.

17b) L.V. Altshuler et al. *Sov. Phys. JETP* **11**, 573 (1960);A.C. Mitchell and W.J. Nellis, *J. Appl. Phys*. **52**, 3363 (1981).

18) A. L. Ruoff et al., *Rev. Sci. Instrum*., **61**, 3830 (1990).

19) H.L. Skriver, *Phys. Rev.*, B **31**, 1909 (1985).

20) D.G. Pettifor, *J. Phys*. **C3**, 367 (1970).

21) J.A. Moriarty, *Phys. Rev.*, B **45**,2004 (1992).

22) J.A. Moriarty, *Phys. Rev.*, B **57**,10340 (1998).

23) P. Oelhafen et al. *J. Phy.:Condens. Matter* **12**, A9 (2000).

24) H. Stupp et al., *J. Non-Cryst. Solids,* **170**, 1 (2000).

25) R. Wahrenberg et al., *Europhys. Lett.* **49**, 782 (2000).

26) J.A. Moriarty, *Phys. Rev.*, B **49**, 12431 (1994).

27) W. Jank, Ch Hausleitner and J. Hafner, *J. Phys.;Condens. Matter,* **3**, 4477 (1991).

28) G. Kresse and J. Hafner, *Phys. Rev*. B **48**, 13115 (1993).

29) A. Pasquarello, et al., *Phys. Rev. Lett***. 69**, 1982 (1992).

30) R. E. Watson and M. Weinert, *Solid State Physics,* **56**, 1 (2001).

31) D.G. Pettifor, *J. Phys.* **F7**, 613 (1977).

32) L. Burakovsky, D.L. Preston and R.R. Silbar, *J. Appl. Phys*. **88**,6294 (2002).

33) R.A. Hixson, et al., *Phys. Rev. Lett***. 62**, 637 (1989).

34) V.V. Brazhkin and A.G. Lyapin, *Physics-Uspekhi,* **43**, 493 (2000).

35) P. Soderlind, et al. *Phys. Rev.* B **57**, 1320 (1998).

36) J.L. Smith and E.A. Kmetko, *J. Less Comm. Metals*, **90**,83 (1989).

37) E.A. Kmetko and H.H. Hill, *J. Phys. F***.** *Metal Phys***. 6**, 1025 (1976).

38) W.H. Zachariasen, *J. Inorg. Nucl. Chem*. **35**, 3487 (1973).

39) B. Johansson and H.L. Skriver, *J. Magn. Magn. Mat.* **29**,217 (1982).

40) G. Bellussi, et al. *J. Less Comm. Metals*, **78**,147 (1981).

41) J.M. Wills and O. Eriksson, *Phys. Rev.* B **45**, 13879 (1992).

42) P. Soderlind et al. *Phys. Rev.* B **52**, 1631 (1995).

43) D. Errandonea, R. Boehler and M. Ross, *Phys. Rev.* B **65**, 012108 (2001).

44) R. Boehler and C-S Zha, *Physica,***139**&**140** B, 233 (1986).

45) H. Olijnyk and W.B. Holzapfel, *Phys. Lett.* A **100**, 191 (1984).

46) A.K. McMahan and J.A. Moriarty, *Phys. Rev.* B **27**, 3235 (1983).

Figure captions

Figure 1. Aluminum melting curve and Hugoniot. DAC measurements [2] (filled circles). Calculated melting curves(solid curves). Calculated solid and liquid Hugoniots (dashed curves), below and above 4700 K repectively. Shock melting points (filled boxes) at melting and freezing pressures determined from breaks in the shock sound velocity. Temperatures at the shock melting points were calculated using the Grüneisen model [17a].

Figure 2. Aluminum Hugoniot. Experimental data (filled circles) [17b]. Hugoniot calculations for solid (solid curve) and liquid (dashed curve).

Figure 3. Molybdenum melting curve and Hugoniot. DAC melting measurements [3] (filled circles). Calculated melting curves; described in text (solid curves). Earlier calculations of Moriarty[21](dashed curve) and Burakovsky[32] (small dashed curve). Calculated Hugoniots: solid (solid curve) and liquid (dashed curves).

Figure 4. Contributions to the excess free energy at a series of temperatures near 75 GPa. $(F^{l}_{th\_inv6} - F^{s}_{th\_inv6})$ and $\Delta U^{l-s}_{d\_band}$ are shown as the solid and small dashed curves. ΔF_{total} is the dashed-dotted curve. Melting occurs at $\Delta F_{\text{total}}=0$.

Figure 5. Calculated DOS for liquid (solid curve) and solid Mo (dashed curve) made at temperatures of 4956 K and 3459 K respectively.

Figure 6. Melting curves of Al [2], Mg[43] and Mo [3]. Near 50 GPa Mg transforms from hcp to bcc [45,46].

Figure 7.Calculated ambient melting temperatures of the "hypothetical light actinides series" (solid curve) and the experimentally determined points plotted as a function of the *f*-electron occupancy (filled circles and dashed curve). The *f*-electron occupancy of the experimental data was taken from the theoretical values reported by Soderlind et al. [42].

Fig. 1

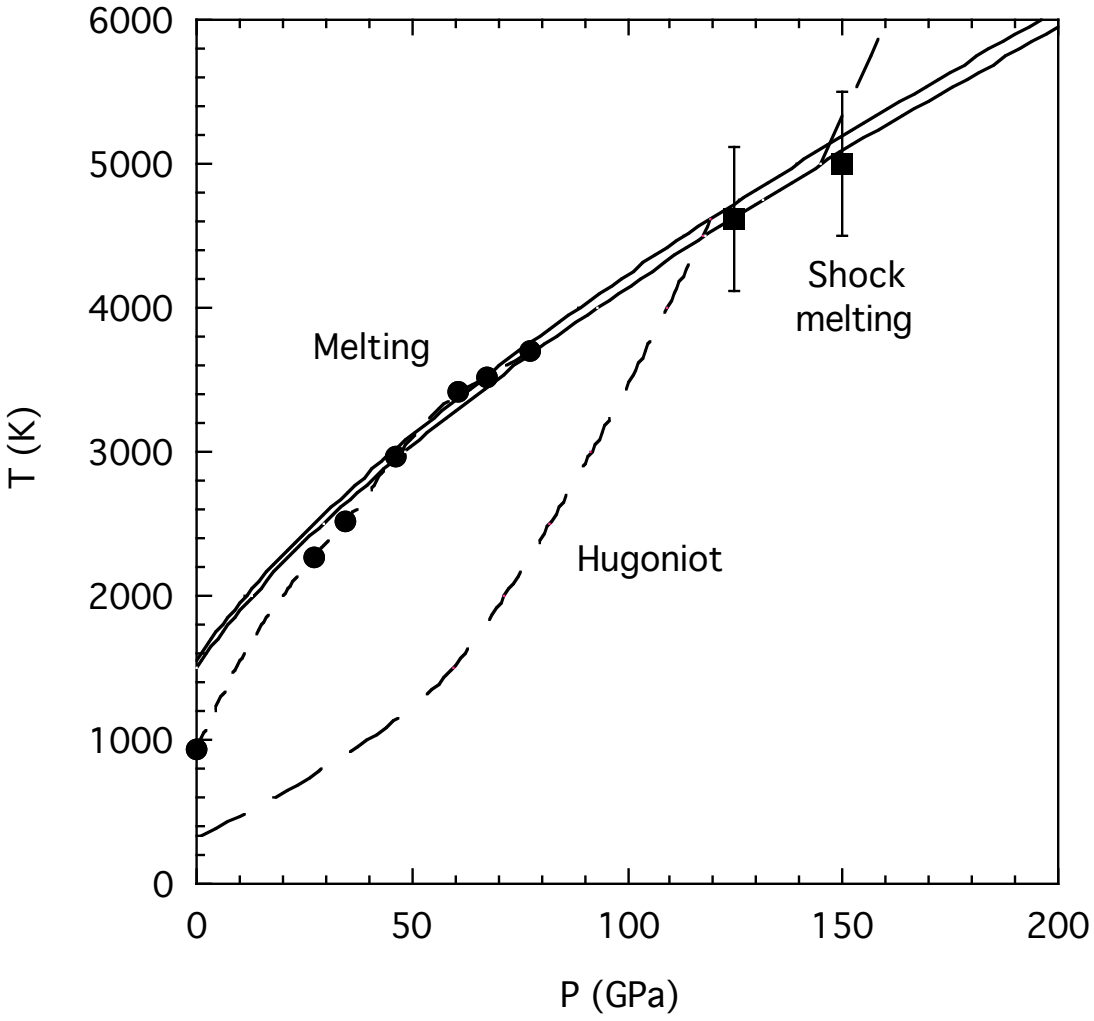
6000
5000
4000
3000
2000
1000
0
T (K)
0
50
100
150
200
P (GPa)
Melting
Shock
melting
Hugoniot

Fig. 2

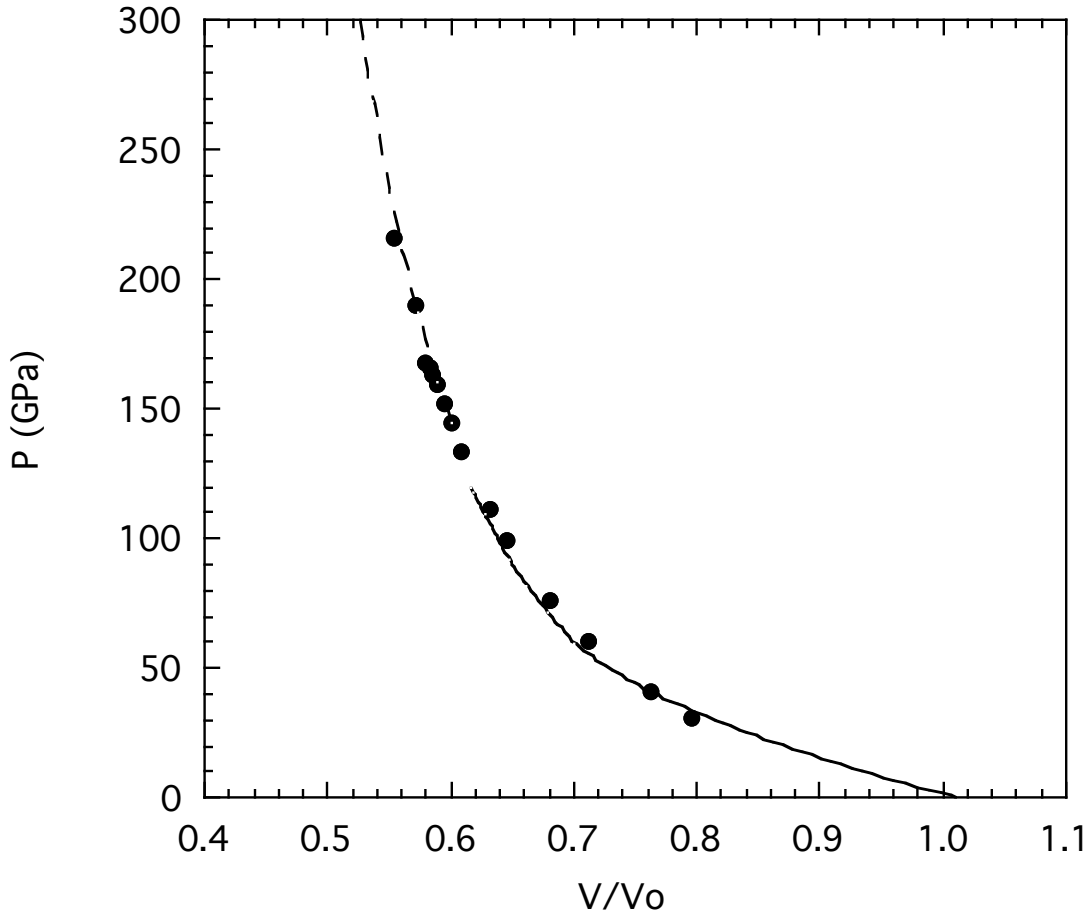

Fig 3

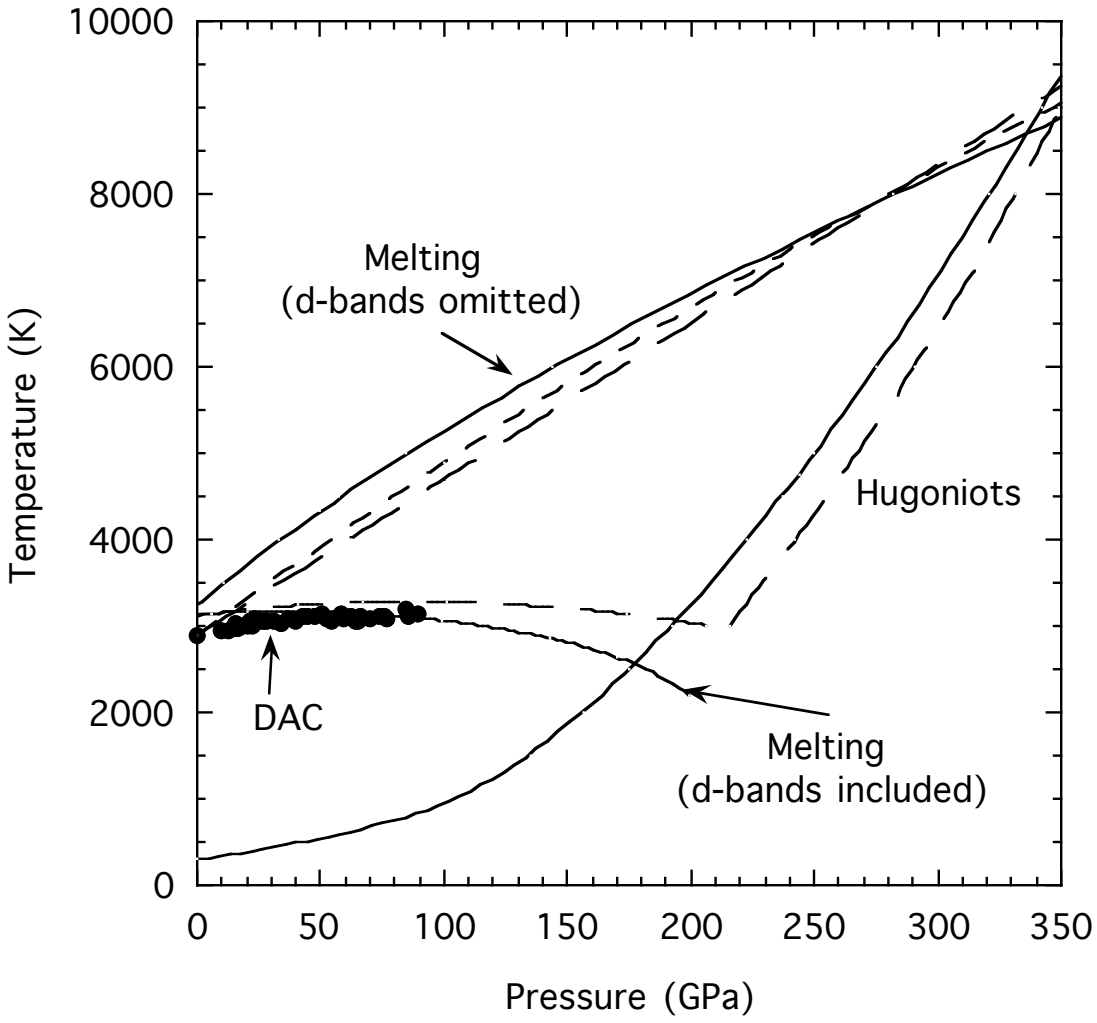
10000
8000
6000
4000
2000
0
Temperature (K)
0
50
100
150
200
250
300
350
Pressure (GPa)
Melting
(d-bands omitted)
Hugoniots
DAC
Melting
(d-bands included)

Fig. 4

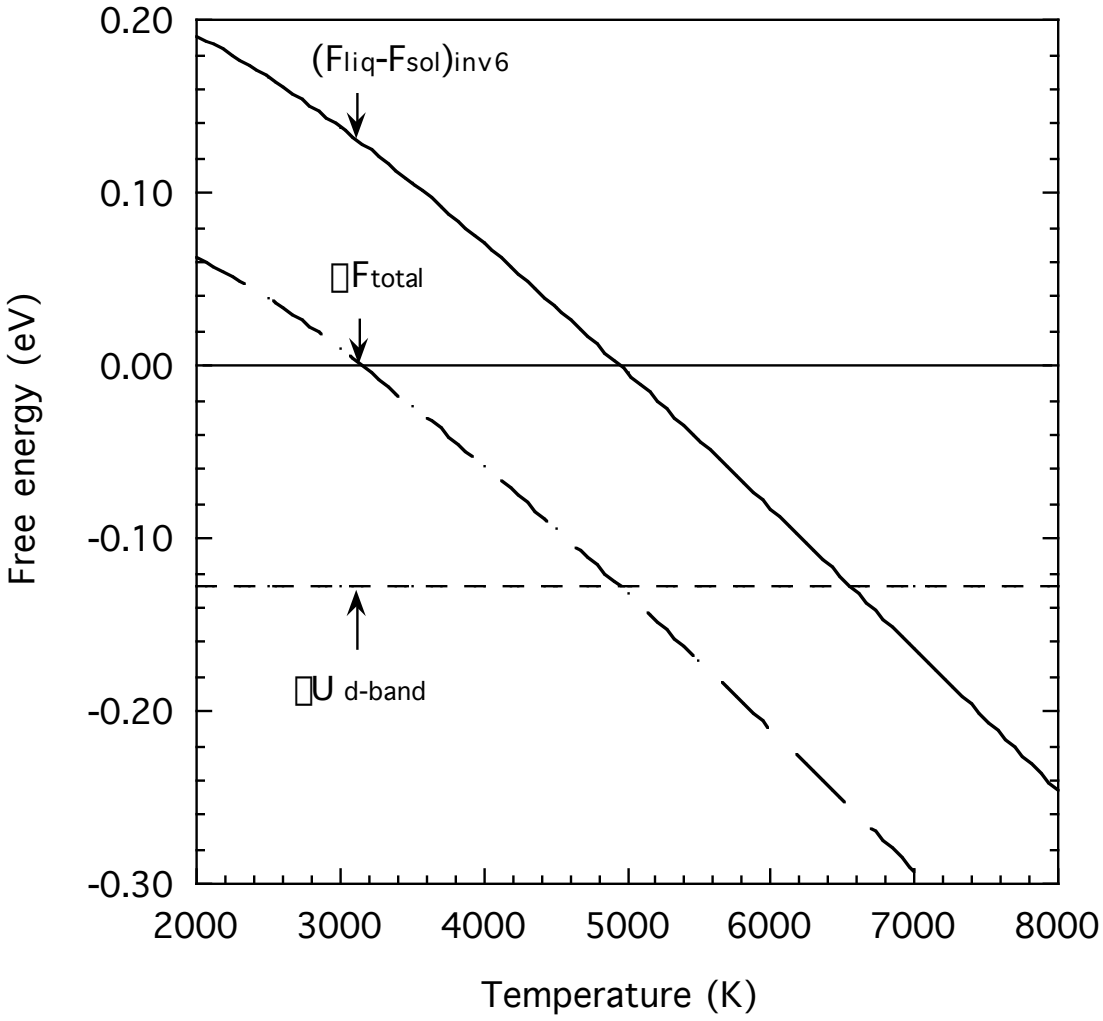
0.20
0.10
0.00
-0.10
-0.20
-0.30
Free energy (eV)
(Fliq-Fsol)inv6
ΔFtotal
ΔU d-band
2000
3000
4000
5000
6000
7000
8000
Temperature (K)

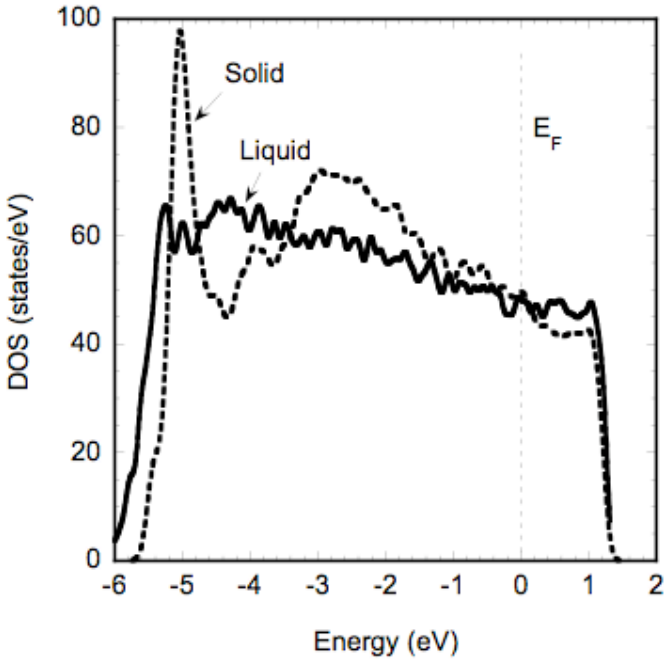
100
80
60
40
20
0
DOS (states/eV)
Solid
Liquid
E_F
-6
-5
-4
-3
-2
-1
0
1
2
Energy (eV)

Fig. 6

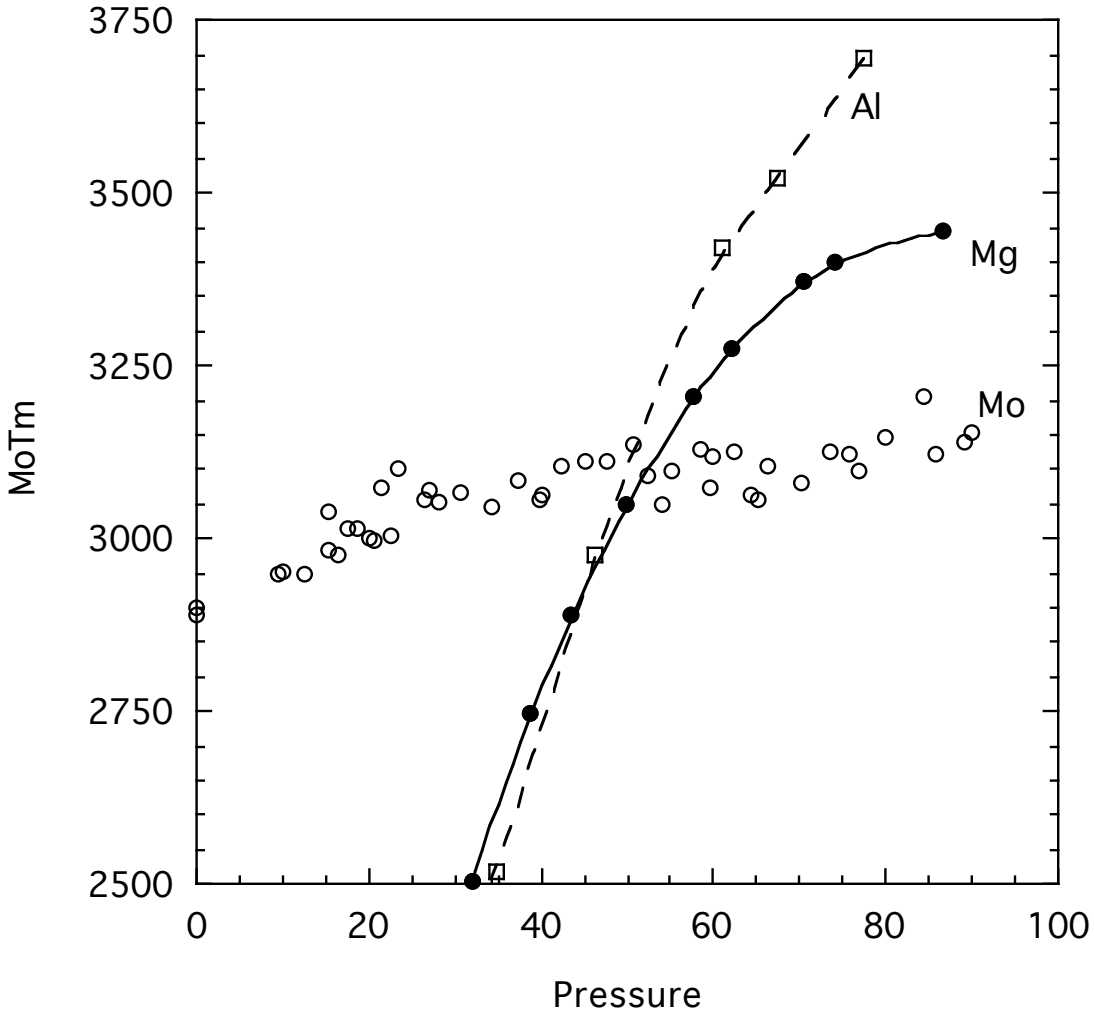
3750
3500
3250
3000
2750
2500
MoTm
0
20
40
60
80
100
Pressure
Al
Mg
Mo

Fig. 7

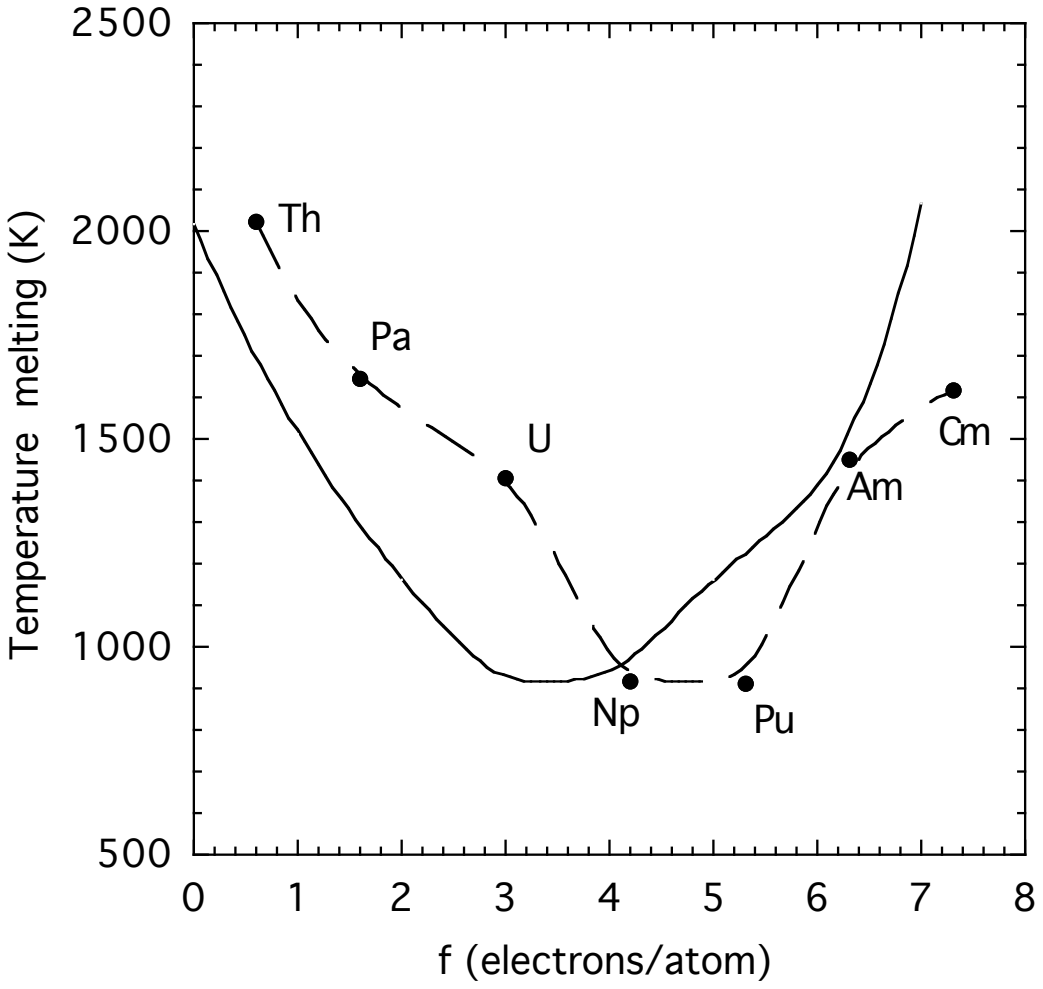
2500
2000
1500
1000
500
Temperature melting (K)
0
1
2
3
4
5
6
7
8
f (electrons/atom)
Th
Pa
U
Np
Pu
Am
Cm